

# Electronic structure depiction of magnetic origin in $\text{BaTiO}_{3-\delta}$ thin film: A combined experimental and first-principles based investigation

Supriyo Majumder<sup>a</sup>, Pooja Basera<sup>b</sup>, Malvika Tripathi<sup>a</sup>, R. J. Choudhary<sup>a,\*</sup>, Saswata Bhattacharya<sup>b,#</sup>, Komal Bapna<sup>c</sup>, and D. M. Phase<sup>a</sup>.

<sup>a</sup>UGC DAE Consortium for Scientific Research, Indore 452001, India

<sup>b</sup>Department of Physics, Indian Institute of Technology Delhi, New Delhi 110016, India

<sup>c</sup>National Physical Laboratory, New Delhi 110012, India

Author(s) to whom correspondence should be addressed. Electronic mail(s): \*ram@csr.res.in, #saswata@physics.iitd.ac.in

With the motive of unraveling the origin of native vacancy induced magnetization in ferroelectric perovskite oxide systems, here we explore the consequences of electronic structure modification in magnetic ordering of oxygen deficient epitaxial  $\text{BaTiO}_{3-\delta}$  thin films. Our adapted methodology employs state-of-the-art experimental approaches viz. photo-emission, photo-absorption spectroscopies, magnetometric measurements duly combined with first principles based theoretical methods within the frame work of density functional theory (DFT and DFT+ $U$ ) calculations. Oxygen vacancy ( $\text{O}_V$ ) is observed leading partial population of Ti 3d ( $t_{2g}$ ), which induces defect state in electronic structure near the Fermi level and reduces the band gap. The oxygen deficient  $\text{BaTiO}_{2.75}$  film reveals Mott-Hubbard insulator characteristic, in contrast to the band gap insulating nature of the stoichiometric  $\text{BaTiO}_3$ . The observed magnetic ordering is attributed to the asymmetric distribution of spin polarized charge density in the vicinity of  $\text{O}_V$  site which originates unequal magnetic moment values at first and second nearest neighboring Ti sites, respectively. Hereby, we present an exclusive method for maneuvering the band gap and on-site electron correlation energy with consequences on magnetic properties of  $\text{BaTiO}_{3-\delta}$  system, which can open a gateway for designing novel single phase multiferroic system.

## I. INTRODUCTION

In oxide systems, the physical and chemical properties are greatly affected by stoichiometry, lattice strain and vacancy induced defect concentrations [1–8]. The fact that mutually exclusive ferroelectricity and ferromagnetism can co-exist in a perovskite ferroelectric system by introducing native vacancies, is of emerging relevance from both technological and fundamental aspects. Owing to the excellent ferroelectric properties,  $\text{Pb}(\text{Zr,Ti})\text{O}_3$  (PZT) thin films have gained tremendous attention till now. However, the toxicity of lead oxide is a major hindrance towards its usage in technological applications [9, 10]. On the other hand lead free  $\text{BaTiO}_3$  (BTO) has emerged as an environment friendly substitute of PZT [9–13] and in addition, promising candidate for the technological demand as capacitors, photo-capacitors, energy storage capacitors, FERAM, optical modulator, electro-optical switch, wave guide [7, 8, 10, 14–19], piezoelectric nanogenerators [20–22], dye-sensitized solar cell electrodes (either in single or in composite form) [23–26], sensors [27] etc.

Various theoretical calculations have predicted that modulating defects generated by creating vacancies at crystal sites can induce magnetic ordering in BTO [28–30]. The magnitude of defect generated magnetization is noticed to be higher for Titanium vacancy in comparison to Oxygen vacancy ( $\text{O}_V$ ) in BTO system [28–30]. However,  $\text{O}_V$  has lower formation energy than Ti vacancy and is a better controllable parameter, offering a suitable pathway to study the induced magnetism in an otherwise non-magnetic BTO.  $\text{O}_V$  can be considered as

self doping process, which effectively acts as additional electron donor in the system, leading to a wide variety of functionalities [7, 8, 19, 31]. Some recent studies demonstrate that nano-crystalline BTO can simultaneously exhibit ferroelectricity and ferromagnetism arising from core and  $\text{O}_V$  at surface of the nano-particles, respectively [32–39]. Despite several research endeavors, the nature and mechanism of induced magnetic ordering is still not properly understood. As it is already transpired by the theoretical predictions that the modification of electronic structure due to  $\text{O}_V$  holds the key to understand the induced magnetism, indeed, a systematic combined experimental and theoretical study is lacking to visualize the alteration in electronic structure caused by  $\text{O}_V$  exclusively.

$\text{O}_V$  can be generated in a very controlled manner while fabricating thin films using pulsed laser deposition (PLD) technique by tuning the oxygen partial pressure (OPP) during the growth process. Here in this work, we elaborate how the  $\text{O}_V$  in epitaxial  $\text{BaTiO}_{2.75}$  thin films significantly modifies the electronic structure across  $E_F$ , reduces the band gap, shows the Mott-Hubbard insulating character, and consequently leads toward the low temperature magnetic ordering, by means of X-ray photoelectron spectroscopy (XPS), valence band spectroscopy (VBS) and X-ray absorption near edge spectroscopy (XANES), magnetometric measurements along with first-principles based spin-resolved density functional theory (DFT and DFT+ $U$ ) calculations.

## II. METHODS

### A. Experimental

*a. Thin film growth and structural characterization:* Epitaxial BTO thin films (thickness  $\sim 150 \text{ nm} \pm 5$ ) are deposited on [001] oriented  $\text{LaAlO}_3$  (LAO) single crystal substrate, by PLD using a KrF excimer laser system (Lambda Physik, wavelength 248 nm, pulse width 20 ns). The single phase stoichiometric bulk target of BTO for thin film growth, is synthesized by conventional solid state reaction method. BTO thin films are grown at different OPP and corresponding nomenclature of films are: BL100 (OPP = 100 mTorr), BL50 (OPP = 50 mTorr) and BL25 (OPP = 25 mTorr). After deposition these films are cooled under same OPP conditions, as used during growth process. Deposition temperature is kept at  $750^\circ\text{C}$  and target to substrate distance is set to 4.5 cm. The laser fluence at the target surface is kept at  $1.8 \text{ J/cm}^2$ . The phase and structural characterization of the films are done by  $\theta - 2\theta$  scans using  $\text{Cu K}\alpha$  ( $\lambda=1.54 \text{ \AA}$ ) X-ray diffraction (Bruker D2 Phaser Desktop Diffractometer). Reciprocal space mapping (RSM) is carried out using high resolution X-ray diffractometer (Bruker D8 Discover HRXRD).

*b. Magnetometric measurements and electronic structure probe:* Magnetization measurements are performed using MPMS 7 Tesla SQUID-VSM (Quantum Design Inc., USA). The chemical valence state of the elements present in the sample are investigated by XPS experiments using  $\text{Al K}\alpha$  lab-source (1486.7 eV) with Omicron energy analyzer (EA-125). For occupied density of states (DOS), valence band spectra (VBS) is recorded at angle integrated photoemission spectroscopy (AIPES) beamline, using synchrotron radiation source (Indus-1, Beam Line 2, RRCAT, Indore, India). Before XPS and VBS measurements, the film surface is cleaned by sputtering using 0.5 keV  $\text{Ar}^+$  ions inside the sample preparation chamber where ultra-high vacuum ( $\sim 10^{-10}$  Torr) is maintained. The charging effect corrections in XPS and Fermi level alignment in VBS, are done by measuring C 1s core level and Au foil (which is in thermal and electrical contact with the sample) VBS, respectively. XPS and VBS spectra are fitted with combined Lorentzian-Gaussian function and Shirley background. Unoccupied DOS is probed by XANES measurements in total electron yield (TEY) mode at O K edge using synchrotron source at soft X-ray absorption spectroscopy (SXAS) beamline (Indus-2, Beam Line 1, RRCAT, Indore, India). All these spectra are recorded at 300 K. The estimated experimental resolutions for VBS and XANES measurements across the measured energy range are about 0.3 eV and 0.25 eV, respectively.

### B. Theoretical

Density functional theory (DFT) calculation is performed using the projector augmented plane-wave (PAW) by employing Vienna ab initio Simulation Package (VASP) [40, 41]. A model structure of  $\text{BaTiO}_3$  consisting of 20 atoms with periodic boundary condition is constructed by  $4 \times 1 \times 1$  replication of the tetragonal  $\text{BaTiO}_3$  unit cell (space group  $P4mm$ ). Several variants of DFT exchange and correlation functionals viz. Local Density Approximation (LDA)[42], Generalized Gradient approximation (GGA) in the form proposed by Perdew, Burke and Ernzerhof (PBE) [43], LDA+ $U$ , GGA+ $U$  (where  $U$  is Hubbard parameter and its value is carefully chosen from experimental inputs) are tested. Due to presence of transition metal in our system, we have employed the DFT+ $U$  approach. The basic idea behind DFT+ $U$  is to treat the strong on-site Coulomb interaction of localized electrons, which is not correctly described by local or semi-local functionals viz. LDA or GGA. It can be described quite accurately at the cost of almost similar computational efforts as with LDA/GGA by involving an additional Hubbard-like term. The on-site Coulomb interactions are particularly strong for localized  $d$  and  $f$  electrons, but can be also important for  $p$  localized orbitals. The strength of the on-site interactions are usually described by parameters  $U$  (on site Coulomb) and  $J$  (on site exchange). These parameters  $U$  and  $J$  can be extracted from ab-initio calculations, but usually are obtained semi-empirically. For  $\text{BaTiO}_3$  system, in order to describe precisely the strong on-site Coulomb repulsion among the localized Ti  $3d$  electrons, we adopt the LDA+ $U$  and GGA+ $U$  formalisms for the exchange correlation term. The equilibrium geometries, band structure, the total and partial density of states (DOS and PDOS) are systematically investigated and analyzed in comparison with experiments and previous calculations. The structure is fully relaxed (both atomic position and cell size) upto 0.001 eV/ $\text{\AA}$  force tolerance using conjugate gradient minimization with  $2 \times 2 \times 2$  K-mesh. The computationally optimized structure details are given in supplementary material (SM). In our calculations, Gaussian smearing is used and the pressure convergence value is set to 0.0001 eV/ $\text{\AA}^3$ . For electronic structure energy calculations, the Brillouin Zone is sampled with a  $8 \times 8 \times 8$  Monkhorst-Pack [44] K-mesh with 0.01 meV energy tolerance. Note that spin-orbit coupling (SOC) is also included while performing the energy calculations. In all our calculations, the plane wave energy cut-off is set to 600 eV.

## III. RESULTS AND DISCUSSION

### A. Structural properties

Figure 1(a) shows the X-ray diffraction  $\theta - 2\theta$  scans of BTO films on LAO substrate, grown at different OPP

values (100, 50 and 25 mTorr). These films are in single phase and [001] oriented. From literature [19, 45], it is known that the BTO films grown by PLD at or above 150 mTorr of OPP, have a stoichiometry close to the ideal value. When these films are deposited at reduced oxygen environment, the films become oxygen deficient [45]. As our prime focus is to investigate the electronic structure and magnetic properties of highest possible oxygen deficient BTO system, we have also deposited thin film at OPP of 5 mTorr. However, its XRD revealed signature of some secondary phase, which could not be indexed with  $\text{BaTiO}_3$ . Therefore, that sample is not considered for further analysis. The calculated in-plane lattice mismatch with the substrate defined as  $(a_{\text{BTO}} - a_{\text{LAO}})/a_{\text{LAO}}$  is  $\sim + 5.36\%$ . Such lattice mismatch will cause in-plane compressive strain in the film during the initial growth stage. From the diffraction pattern, it can be noted that the [001] peak shifts towards smaller  $2\theta$  values with decreasing OPP. This suggests the increment of the out-of-plane lattice parameter with the decrease of OPP during growth of BTO thin film.

To obtain the nature of substrate induced strain present in the film, RSM around asymmetric (103) reflection is performed, as shown in Fig.1(b) for samples BL25 and BL50. It is clear from these RSM plots that both of the films are epitaxial in nature. Here the  $q_x$  and  $q_z$  axis correspond to the in-plane and out-of-plane directions, respectively. Let  $(q_{xf}, q_{zf})$  and  $(q_{xs}, q_{zs})$  denote the maximum intensity coordinates for the film and substrate, respectively. In both the cases  $(q_{xf}, q_{zf})$  is sufficiently shifted from  $(q_{xs}, q_{zs})$ , indicating that the films are relaxed. The large lattice mismatch ( $\sim + 5.36\%$ ) between bulk BTO and LAO substrate and a thickness higher than the critical one to sustain substrate induced strain, may be the possible reason for such strain relaxation. The in-plane lattice parameter 'a' calculated from  $q_{xf}$ , for both the films are found close to the BTO bulk in-plane lattice parameter value. But, the  $q_{zf}$  values of BL50 is significantly higher than the  $q_{zf}$  value corresponding to BL25, suggesting an increase of out-of-plane lattice parameter 'c' with decrease in OPP. In reduced oxygen environment O vacancies created in BTO films are compensated by lowering the oxidation state of some Ti ions from 4+ to 3+ (as shown later). The presence of  $\text{Ti}^{3+}$  may be the possible reason for such elongation of out-of-plane lattice parameter (c), as  $\text{Ti}^{3+}$  has larger ionic radius than  $\text{Ti}^{4+}$ .

## B. Electronic properties

### 1. Chemical valence state

For the electronic structure studies, we chose BL25 sample which was deposited in single phase under lowest OPP and hence should possess maximum  $\text{O}_V$  defect states among the grown films. To investigate the effect of oxygen deficiency in chemical valence state of

the elements, we have performed XPS measurements of BL25 sample which is shown in Fig.2(a, b). Deconvolution of the O 1s XPS spectra in Fig.2(a) indicates the presence of three possible features having binding energies centered at 529.8, 531.5 and 533.3 eV, which are attributed to lattice oxygen ( $\text{O}_L$ ) bound to Ti, O vacancies or defects ( $\text{O}_V$ ) and the combined chemisorbed oxygen ( $\text{O}_C$ ) species, respectively [46]. The core lines of Ti 2p are split into  $2p_{3/2}$  and  $2p_{1/2}$  due to spin orbit interaction, (Fig.2(b)) which can be deconvoluted by fitting the spectrum with peaks contribution from both  $\text{Ti}^{3+}$  and  $\text{Ti}^{4+}$  states, centered at binding energies 457.0 eV ( $\text{Ti}^{3+} 2p_{3/2}$ ), 462.6 eV ( $\text{Ti}^{3+} 2p_{1/2}$ ), 458.7 eV ( $\text{Ti}^{4+} 2p_{3/2}$ ) and 464.4 eV ( $\text{Ti}^{4+} 2p_{1/2}$ ), respectively [47]. From these XPS data it can be concluded that as expected, the BL25 film is highly oxygen deficient and these O vacancies are compensated by lowering the oxidation state of some Ti atoms, from 4+ to 3+. It is also noticed that the integrated intensity of  $\text{Ti}^{3+}$  state is very close to  $\text{Ti}^{4+}$  state and on average these XPS data reveal that the  $\text{Ti}^{4+} : \text{Ti}^{3+}$  content is in 1 : 1 ratio. Thus the effective chemical formula of BL25 sample will be;  $[\{ \text{Ba}(\text{Ti}_x^{4+}\text{Ti}_{1-x}^{3+})\text{O}_{3-\delta} \}]$ , such that  $x \approx (1-x)$  and  $x+2\delta-1 \approx 0$   $\cong \text{Ba}(\text{Ti}_{0.5}^{4+}\text{Ti}_{0.5}^{3+})\text{O}_{2.75}$  which will yield,  $\text{BaTi}^{3.5+}\text{O}_{2.75}$  with  $\delta = 0.25$ . This stoichiometry is maintained across the thickness as confirmed from the depth dependent XPS measurements (not shown here).

### 2. Valence band spectroscopy

To analyze the occupied density of states near Fermi level, valence band spectroscopy measurements were performed. Figure 2(c) shows the fitted VBS of BL25 recorded at incident photon energy of 45 eV. Deconvolution of this VB spectra reveals the four features A, B, C and D centered at binding energies 1.5, 4.7, 6.4 and 7.7 eV, respectively [48]. The feature B is assigned as O 2p - O 2p non-bonding states, while features C and D are ascribed to Ti 3d - O 2p bonding  $dp\sigma$  and  $dp\pi$  states, respectively [49]. Feature A has been attributed to  $\text{Ti}^{3+} 3d$  defect state [47, 49, 50]. It should be noted that feature A is not observed in the VBS of stoichiometric  $\text{BaTiO}_3$  [48]. Therefore, the observance of feature A can be assigned to the presence of oxygen vacancies. O vacancy causes partial change in band filling from  $d^0$  (in stoichiometric  $\text{BaTiO}_3$ :  $\text{Ti}^{4+}$ ) to  $d^1$  (partially populated 3d in  $\text{BaTiO}_{3-\delta}$ : mixed  $\text{Ti}^{3+}$  &  $\text{Ti}^{4+}$ ), which causes the appearance of new feature A near Fermi level.

### 3. X-ray absorption near edge spectroscopy

To probe the unoccupied electronic density of states of these oxygen deficient films, we have performed X-ray absorption near edge spectra measurements at the O K edge as shown in Fig.2(d), which gives information about the hybridization of transition metal and oxygen states

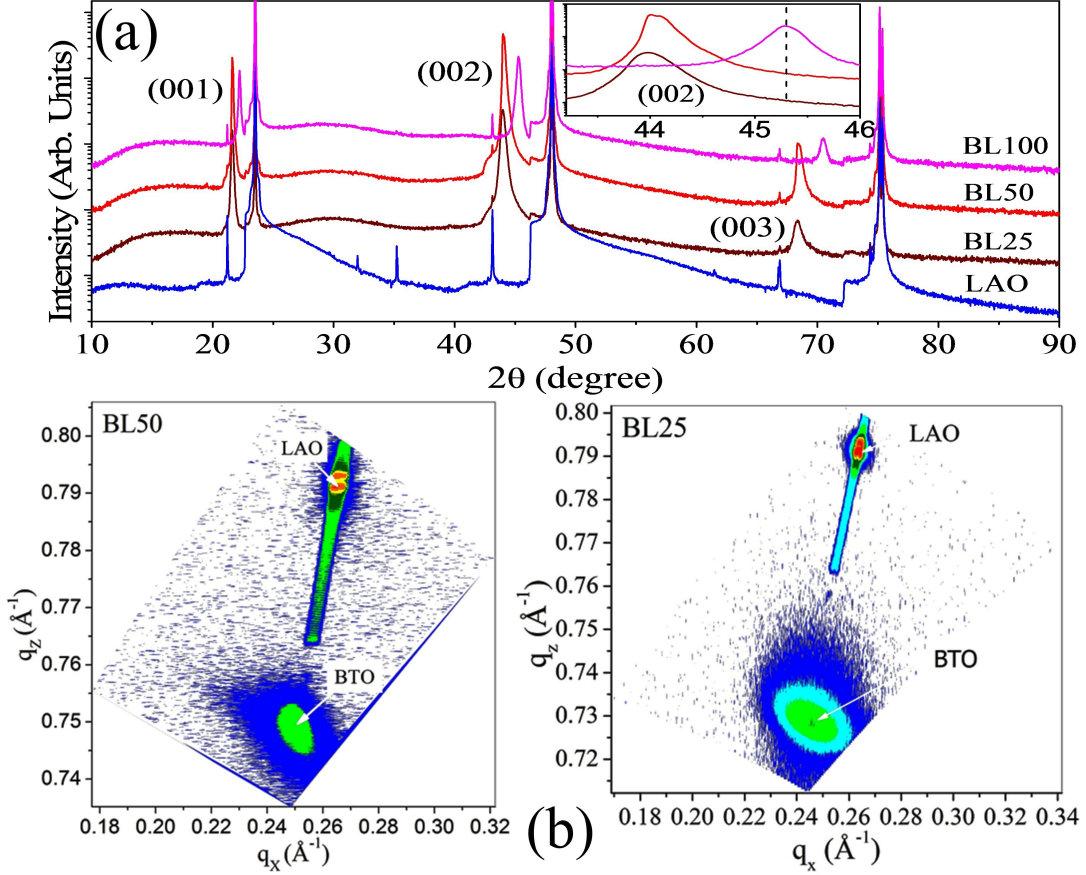


FIG. 1. (a): XRD ( $\theta - 2\theta$ ) patterns of BTO thin films deposited at different oxygen partial pressures on (001) LAO substrate along with the (001) LAO substrate, inset displays the (002) peak of BTO films. (b): Reciprocal space maps around asymmetric (103) plane of BTO/LAO films. Arrows show the most intense coordinates in ( $q_x$ ,  $q_z$ ) domain correspond to BTO film and LAO substrate.

[51]. For comparison we have also measured XANES of BTO single crystal. The features marked by A, B and C in Fig.2(d) correspond to the hybridized states between O 2p and Ti 3d, while feature D is assigned to O 2p derived states hybridized with Ba 5d [52]. Feature E can be identified as excitation from Ti 4sp - O 2p [53]. The two peaks labelled as A and B can be identified as  $t_{2g}$  and  $e_g$  bands, respectively [51] arising due to crystal field splitting.

It is observed that the intensity ratio of  $t_{2g}$  related feature (A) with  $e_g$  feature (B) varies as,  $I(t_{2g})/I(e_g):BTO \text{ single crystal} > I(t_{2g})/I(e_g):BL50 > I(t_{2g})/I(e_g):BL25$ . In general the intensity ratio of  $t_{2g}$  and  $e_g$  can be considered as a rough estimate of  $d$  electron count [51]. O vacancy induced doped electrons start filling empty  $t_{2g}$  (Ti 3d) orbitals and as a result the number of unoccupied states reduces. This is further confirmed by reduction in  $I(t_{2g})/I(e_g)$  intensity ratio with increasing O vacancies. The intensity ratio  $I(t_{2g})/I(e_g)$  is also related to hybridization strength [51]. The drop of intensity ratio  $I(t_{2g})/I(e_g)$  indicates that the hybridization between Ti 3d and O 2p decreases with increasing O vacancies. It should be noted that O vacancy induces

a reduction in Ti valence state. Lowering the oxidation states leads to the increase in charge transfer energy  $\Delta$  [54]. Thus the higher oxygen deficient films with higher  $Ti^{3+}$  content should show weaker hybridization between Ti 3d and O 2p, since the hybridization strength is inversely proportional to  $\Delta$  [53], which is reflected in the XANES result.

#### 4. Electronic structure near Fermi level

Finally, using XPS O 1s core level binding energy, the VBS and XANES spectra are brought to common energy scale [55], to get a schematic of electronic band structure (shown in Fig.3) of BL25 sample. It is known that the stoichiometric  $BaTiO_3$  is a band-gap (3.2 eV) insulator [56]. However, in  $BaTiO_{3-\delta}$  thin film, as evident from Fig.??, due to O vacancies, the overall electronic structure is greatly modified across the Fermi level. The presence of  $Ti^{3+}$  3d defect state in band structure near the Fermi level causes a reduction in the band gap (from 3.2 eV to  $\sim 1.8$  eV). The estimated band width of this metal 3d defect feature is about  $W = 1.4$  eV. From



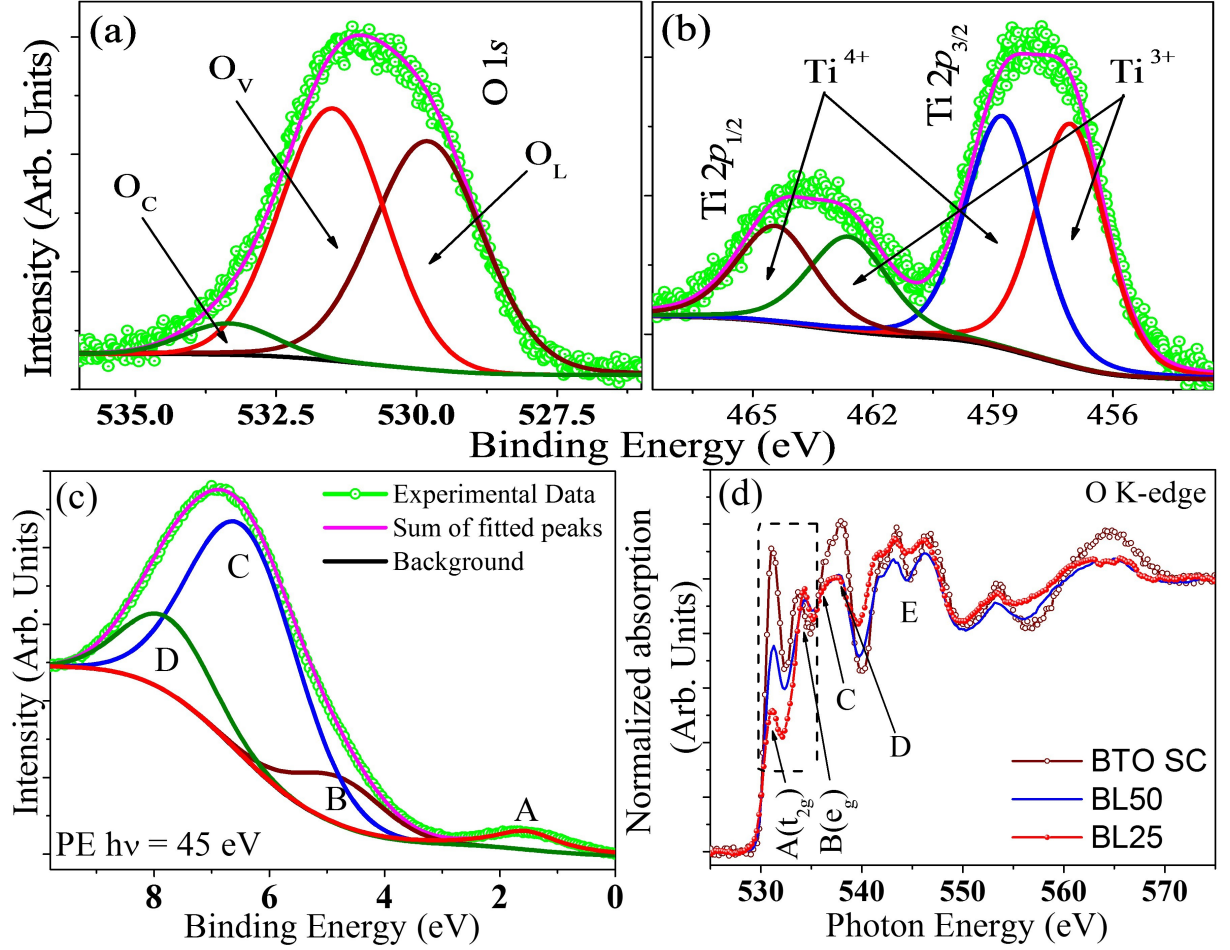


FIG. 2. XPS spectra of BL25 film, (a): O 1s, indicating the presence of three types of oxygen,  $O_L$ ,  $O_V$  and  $O_C$  (see text); (b): Ti 2p, indicating the presence of both  $Ti^{4+}$  and  $Ti^{3+}$  states. (c): Valence band spectra of BL25 recorded at photon energy of  $h\nu=45$  eV. (d): O K edge XANES spectra recorded at TEY mode for BTO single crystal, BL50 and BL25 samples.

this electronic structure, the  $Ti^{3+}$  3d defect state in the valence band and the Ti 3d  $t_{2g}$  feature in conduction band can be identified as the spectroscopic signature of lower Hubbard band (LHB) and upper Hubbard band (UHB), respectively. From the energy separation between the UHB and LHB, we have estimated the on-site  $d-d$  Coulomb interaction energy  $U$  to be approximately equal to 3 eV[57]. Similarly, the ligand to metal charge transfer energy  $\Delta$ , can be estimated as the energy difference in UHB and O 2p band [57] and it takes a value of about 6 eV in our system. Here we have observed  $U/W > 1$  and  $U < \Delta$ , thus the oxygen deficient  $BaTiO_{3-\delta}$  system should be categorized as a Mott-Hubbard type insulator. The resistivity behavior (SM, Fig.S3) confirms that the increase in  $O_V$  concentration increases the conductivity, even-though the system remains insulating in nature.

### C. Magnetic properties

Now to study the effect of O vacancy on the magnetic properties of  $BaTiO_{3-\delta}$  system, we have performed dc magnetization measurements. Figure 4(a) shows the  $M(T)$  curves in field-cooled warming (FCW) mode in presence of  $\mu_0 H = 100$  Oe applied magnetic field in a direction parallel to the surface of the film. In order to estimate the ordering temperature, here we have determined inflection temperature point in temperature derivative of magnetization, which is an indication of magnetic transition [58, 59]. As shown in the inset of Fig.4(a), the derivative of magnetization with respect to temperature ( $\frac{dM}{dT}$ ) has the minima at  $T \approx 43.9$  K for BL25 and 42.3 K for BL50. Therefore, we have considered the magnetic transition temperatures as 43.9 K and 42.3 K for BL25 and BL50, respectively. The change in the  $O_V$  concentration significantly affects the magnetic moment values but the ordering temperatures do not change as such. The magnetic transition temperature does not show any sig-

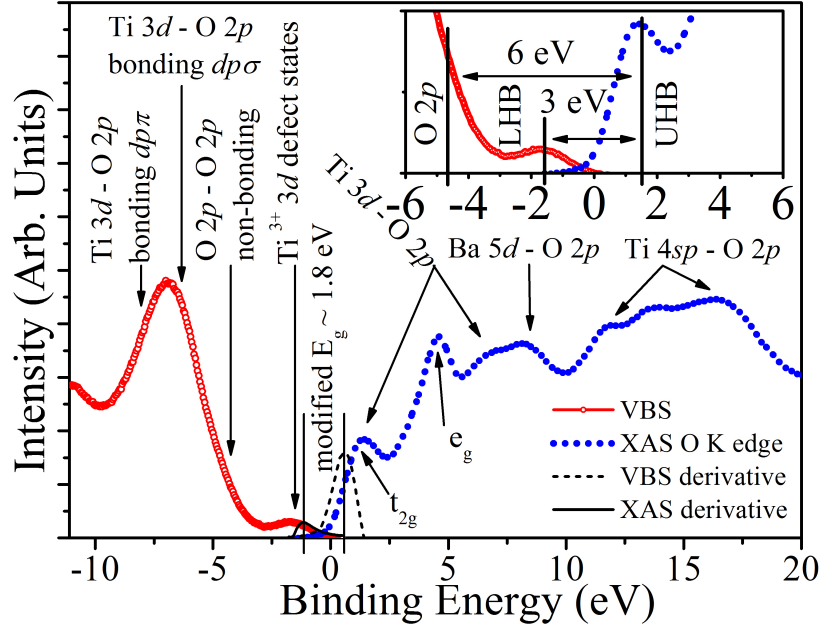


FIG. 3. Schematic electronic band structure of BL25 film. The presence of band gap defect state modifies the band gap and electronic structure of the system. Inset shows the estimated  $U$  and  $\Delta$  (see text).

nificant field dependency (SM, Fig.S1), but as expected, the magnetic moment value increases with increasing the measuring magnetic field. It should be noted that no anomalous magnetic ordering is observed when we repeated the same measurement with stoichiometric single crystal (SC) of BTO. With decreasing OPP the  $O_V$  and  $O_V$  induced  $Ti^{3+}$  concentrations in the films increase. As the magnetic moment is contributed from these  $O_V$  induced  $Ti^{3+}$ , the BL25 thin film shows moment value one order higher than BL50. To ascertain the hysteric nature of these  $BaTiO_{3-\delta}$  thin films,  $M(H)$  isotherms were collected at different temperatures, as shown in Fig.4(b). The diamagnetic contribution from the substrate is generated from extrapolating the high filed linear part of  $M(H)$  curves and subtracted with the overall magnetic moment. Finite value of coercivity ( $H_c \sim 200$  Oe) is observed for both of the films. As the minor impurities in substrates may also cause some unexpected magnetic ordering, we have also performed magnetization measurements of bare LAO substrate (SM, Fig.S2) treated under identical thermal and vacuum conditions which were used for film (BL25) fabrication. The magnetization behaviors of the substrate show typical dia-magnetic nature, confirming the observed magnetic results of BTO/LAO samples are intrinsic magnetic properties of  $BaTiO_{3-\delta}$  system. As expected, BL25 ( $M_S \sim 0.57 \mu B/f.u.$ ) shows much higher saturation magnetization than BL50 ( $M_S \sim 0.27 \mu B/f.u.$ ).

As discussed earlier, there are lot of debates regarding the localization of two free electrons generated by the formation of one O vacancy. Cao *et al.*[29], suggested that O vacancy induced magnetic moment in bulk  $BaTiO_3$  arises from unpaired electrons at neighboring

of  $Ti t_{2g}$  states. According to first principles calculations based on GGA formalism in ref. Cao *et al.* 2009[29], O vacancy mediated magnetic moments at nearest and second nearest neighbors of Ti atoms are about  $0.22-0.28 \mu B$  and  $0.06-0.09 \mu B$ , respectively, which give rise a total magnetic moment of about  $1.27-1.54 \mu B$  in tetragonal phase of  $BaTiO_3$ . In another theoretical report Cao *et al.*[30] also studied the effect of O vacancies on magnetic properties of (001) cubic  $BaTiO_3$  thin film using DFT calculations and claimed that the O vacancy in Ba-O terminated surface can cause magnetism which is due to the spin-polarization of electrons localized at vacancy basin. The GGA+ $U$  calculations in ref. Cao *et al.* 2011[30] showed that the presence of O vacancies can induce magnetic moment about  $1.12 \mu B$  (with  $U = 0$ ) and  $1.93 \mu B$  (with  $U = 3$  eV). Whereas, Raelarijaona *et al.*[28], showed that O vacancy induced magnetization in bulk BTO have its origin in the spin polarization of the itinerant electrons at  $Ti 3d (t_{2g})$  orbitals. The LDA+ $U$  calculations for different  $U$  in ref. Raelarijaona *et al.* 2017[28], yield the magnetic moment value  $0.25$ ,  $0.5$  and  $1.5 \mu B$  for  $U = 0, 3$  and  $6$ , respectively. All these reports claim that ferromagnetism is energetically more favorable than antiferromagnetism in O deficient  $BaTiO_{3-\delta}$  system.

From the electronic structure it is evident that O vacancy leads to modification in VB as well as variation in feature related  $Ti 3d t_{2g}$  state in the conduction band. This clearly underlines that O vacancy results in occupancy of  $3d$  states of neighboring Ti atoms converting them from  $Ti^{4+}$  to  $Ti^{3+}$ . In the crystal structure of BTO, an O atom is shared between two neighboring Ti atoms. If both these Ti atoms accept an electron each

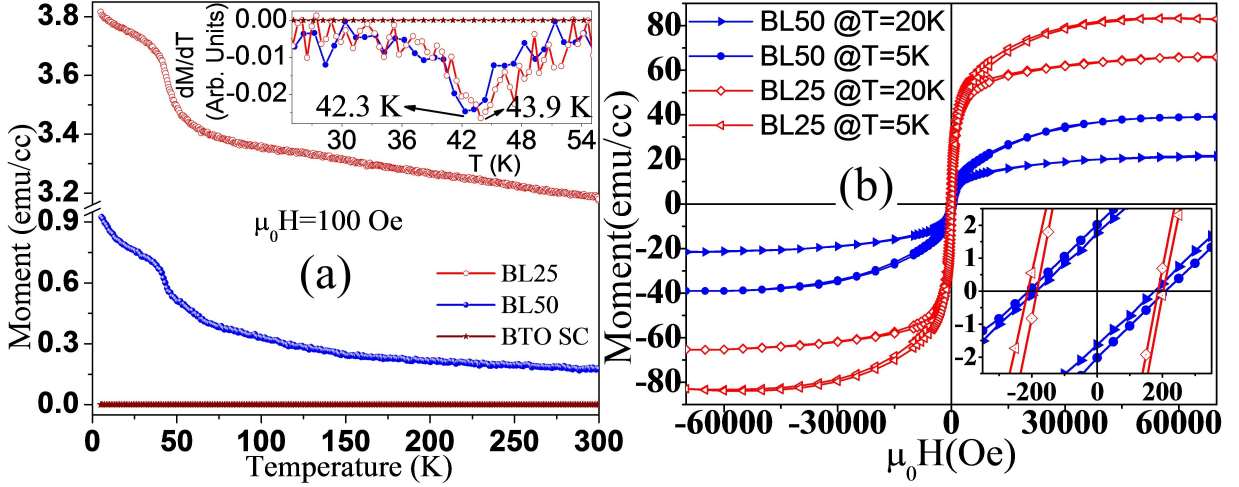


FIG. 4. (a): FCW cycle of  $M(T)$  curves at applied magnetic field 100 Oe. Inset shows magnetization derivative as a function of temperature. (b):  $M$ - $H$  isotherms measured at 20 K and 5 K temperatures.

due to O vacancy, they will be converted into  $\text{Ti}^{3+}$ . It is shown in previous studies that  $\text{Ti}^{3+}\text{O}^{2-}\text{Ti}^{3+}$  exchange interactions display antiferromagnetic ordering [60, 61]. However, in the present study the observed magnetic properties preclude such possibility of collinear antiferromagnetism. Thus it is quite reasonable to assume that in the present case most of the electrons available due to O vacancies are localized at the adjacent Ti site, transforming them from  $\text{Ti}^{4+}$  to  $\text{Ti}^{3+}$ , whereas some of them are also distributed at next Ti atoms. This will create an asymmetric charge distribution at Ti sites in proximity of O vacancy, viz.  $\text{Ti}^{4-\epsilon}\text{-O-Ti}^{3+\epsilon}\text{-O}_V\text{-Ti}^{3+\epsilon}\text{-O-Ti}^{4-\epsilon}$  chains. The exchange interaction between these local moments will lead to magnetic ordering with uncompensated magnetization. O vacancy in BTO induced n-type carrier doping (as discussed later). Such defect carriers mediate the magnetic interactions by forming bound magnetic polaron (BMP) [62, 63] with local magnetic moment due to  $\text{Ti}^{3+}$ . Depending on the carrier concentration and magnetic impurity concentration, such BMPs overlap and lead to long range magnetic ordering between  $\text{Ti}^{4-\epsilon}$  and  $\text{Ti}^{3+\epsilon}$  ions. As the O vacancy concentration increases, more number of bound magnetic polarons are formed yielding a larger value of magnetic moment with increasing O vacancy.

#### D. First principles calculations

The DFT calculation is carried out on  $\text{BaTiO}_3$  (stoichiometric) and  $\text{BaTiO}_{2.75}$  (oxygen deficient) system. For simulation of  $\text{BaTiO}_{2.75}$  composition, one oxygen atom is removed from the center of the supercell (Fig.5(a)). To get a better insight we have used DFT+ $U$  approach with  $U = 3$  eV, which was estimated from present spectroscopic observations (shown in Fig.3). This on-site Coulomb interaction  $U$  is added to Ti site. The-

oretically calculated band structure of  $\text{BaTiO}_{2.75}$  system using LDA+ $U$  and GGA+ $U$  formalism are shown in Fig.5(b, c). For band structure we have plotted the Kohn-Sham energy eigenvalues calculated along the high symmetry path i.e.,  $\Gamma$  (0 0 0), M (0.5 0.5 0), X (0.5 0 0),  $\Gamma$  (0 0 0), A (0.5 0.5 0.5), R (0.5 0 0.5), Z (0 0 0.5). The DFT band gap of the stoichiometric  $\text{BaTiO}_3$  (tetragonal  $P4mm$ ) is  $\sim 1.78$  eV from LDA and  $\sim 2.8$  eV from GGA approaches (DFT underestimates the band gap), which is in agreement with previous calculations [64]. It is observed that O vacancy induces modification in the band structure and reduces the band gap of the system as compared to the stoichiometric case. Fig.6(a) (LDA, LDA+ $U$  scheme) and Fig.6(b) (GGA, GGA+ $U$  scheme) depict the simulated total and partial density of states (PDOS) for the stoichiometric and oxygen deficient BTO system. Comparing the stoichiometric and oxygen deficient case, one can identify some noticeable features, as following: (i) the presence of defect states in PDOS of Ti 3d (very near to the Fermi energy) changes the overall DOS of the system and the orbital-resolved DOS of Ti (not shown here) confirms that these states consist of Ti 3d  $t_{2g}$  orbitals, (ii) O vacancy causes a reduction in band gap of the system, and (iii) O vacancy leads to n-type doping in the system. These findings are well consistent with our experimental outcomes.

To understand the origin of magnetism, we have performed spin-resolved DFT calculations on stoichiometric  $\text{BaTiO}_3$  and oxygen vacant  $\text{BaTiO}_{2.75}$  compositions. The spin-resolved density of states near the Fermi energy level are plotted in Fig.6(c) and Fig.6(d) for different theoretical schemes LDA, LDA+ $U$ , GGA and GGA+ $U$ . Here, the spin-up and spin-down components are shown in positive and negative scale, respectively. Both of our LDA and GGA calculations show identical spin-up and spin-down DOS component for stoichiometric  $\text{BaTiO}_3$  system, resulting a vanishing magnetic moment value. By focusing



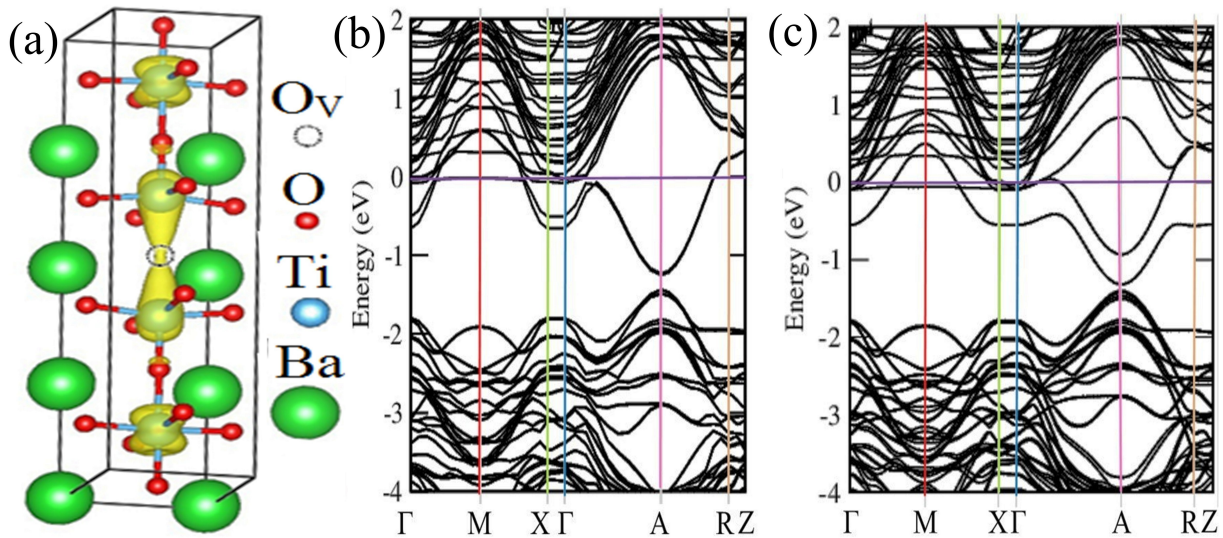


FIG. 5. (a): Spatial distribution of spin polarized charge density around oxygen vacancy in  $\text{BaTiO}_{2.75}$  supercell. Electronic band structures of  $\text{BaTiO}_{2.75}$  composition simulated using; (b): LDA+ $U$ , (c): GGA+ $U$  functionals.

on the spin-resolved DOS obtained from LDA, LDA+ $U$ , GGA and GGA+ $U$  formalisms for  $\text{BaTiO}_{2.75}$  composition, one can clearly identify that here spin-up and spin-down DOS components are not symmetric i.e. they are spin-polarized. This spin polarization induces magnetism in oxygen deficient  $\text{BaTiO}_{2.75}$  system. Inclusion of on-site Coulomb interaction  $U$  in spin resolved DFT+ $U$  calculations, results in more asymmetry in spin-up and spin-down DOS i.e. DFT+ $U$  calculations yield higher magnetization.

To investigate the issue of charge localization induced by oxygen vacancy we have studied the spatial distribution of spin polarized charge density around the oxygen vacancy site (shown in Fig.5(a)) in  $\text{BaTiO}_{2.75}$  composition. Figure 5(a) shows that the spin polarized charge density is mostly spread at first nearest neighbor (FNN) Ti sites adjacent to the oxygen vacancy. A small part of the spin polarized charge density is also distributed at second nearest neighbor (SNN) Ti atoms. From GGA+ $U$  approach we have found that magnetic moment in  $\text{BaTiO}_{2.75}$  is originating from FNN and SNN Ti atoms neighboring to the oxygen vacancy and the calculated values of magnetic moments at FNN and SNN Ti sites are about,  $0.44\mu_B$  and  $0.12\mu_B$ , respectively. These results further confirm our prediction of asymmetric charge distribution at Ti sites in the proximity of oxygen vacancy, which leads to asymmetric distribution of magnetic moment values. After creating oxygen vacancy, the lattice was allowed to relax around the vacancy site. We have found that Ti atoms adjacent to the oxygen vacancy site goes away from each other due to coulomb repulsion and as a result of this the supercell gets elongated (shown in Fig.5(a)). Oxygen vacancy induced charge imbalance is compensated by lowering the valence state of adjacent Ti atoms. The lower valency Ti ions having larger ionic radius will push away each other

by coulomb repulsion. This is also corroborated by the elongated lattice parameter as observed from XRD and RSM analysis (shown in Fig.1).

From the aforementioned discussions, it is transpired that the oxygen vacancy greatly modifies the electronic structure of BTO. These modifications in electronic structure have huge bearings on the magnetic properties. It is observed that oxygen vacancy leads to (i) n-type doping in the system, (ii) partial occupancy of Ti  $3d$   $t_{2g}$  states, (iii) reduction in band gap, (iv) change in insulating nature from band gap to Mott-Hubbard with on-site  $d-d$  Coulomb repulsion energy  $U$  being 3 eV, (v) induce magnetic ordering, (vi) formation of spin-polarized states near the Fermi energy level, (vii) inclusion of  $U$  in DFT+ $U$  calculations causes more spin-polarization in spin resolved DOS components and (viii) asymmetric distribution of spin-polarized charge densities at FNN and SNN Ti sites adjacent to the  $\text{O}_V$ .

#### IV. CONCLUSION

In summary, we have investigated the oxygen vacancy ( $\text{O}_V$ ) induced modifications in electronic structure on  $\text{BaTiO}_{3-\delta}$  thin film system, using combined experimental and theoretical tools to interpret the origin of magnetic ordering.  $\text{O}_V$  related charge imbalances are compensated by lowering the oxidation state of some Ti atoms from 4+ to 3+ states. Both of our experimental and theoretical investigation confirm partial population of Ti  $3d$   $t_{2g}$  state in  $\text{BaTiO}_{3-\delta}$  system, which modifies the electronic structure across the Fermi level resulting a reduction in band gap of the system. By estimating  $d-d$  Coulomb interaction energy  $U$  and ligand to metal charge transfer energy

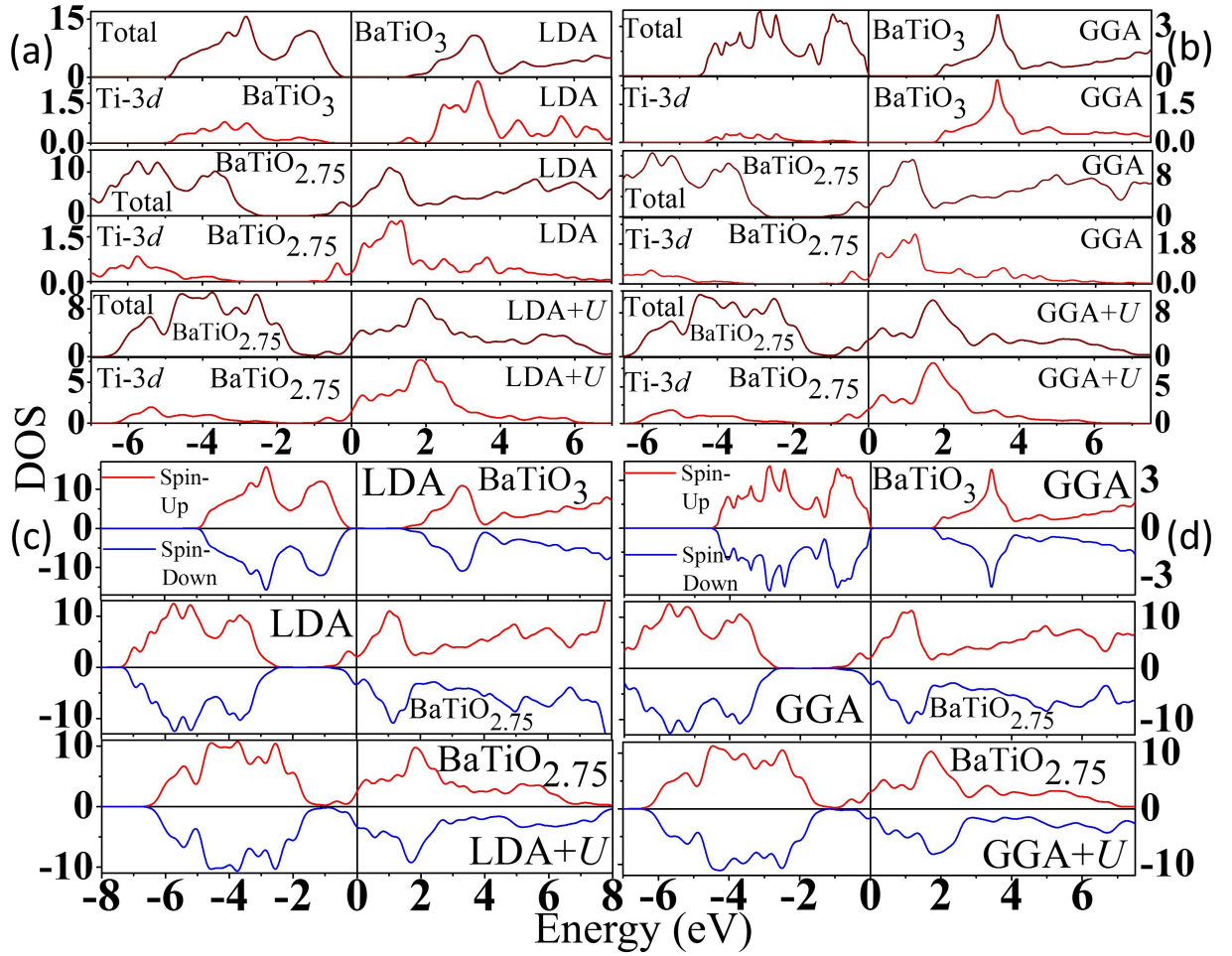


FIG. 6. Total and partial (Ti-3d) DOS near the Fermi level for  $\text{BaTiO}_3$  and  $\text{BaTiO}_{2.75}$  compositions calculated using; (a): LDA and LDA+ $U$  functionals, (b): GGA and GGA+ $U$  functionals. Spin-resolved DOS near the Fermi level simulated using; (c): LDA and LDA+ $U$  functionals, (d): GGA and GGA+ $U$  functionals.

$\Delta$ , we have categorized the oxygen deficient  $\text{BaTiO}_{2.75}$  as a Mott-Hubbard insulator. Bulk magneto-metric study reveals that oxygen vacancy induces anomalous magnetic ordering in  $\text{BaTiO}_{3-\delta}$  thin film systems. On the basis of observed signatures of the asymmetric charge distribution in the vicinity of  $\text{O}_V$  site, we have explained the intriguing magnetic ordering in  $\text{BaTiO}_{3-\delta}$  thin films accounting the interaction of  $\text{Ti}^{4-\epsilon}-\text{O}-\text{Ti}^{3+\epsilon}-\text{O}_V-\text{Ti}^{3+\epsilon}-\text{O}-\text{Ti}^{4-\epsilon}$  chains. The spin resolved density of states and spatial distribution of spin polarized charge density in the proximity of the vacancy site confirm our interpretation regarding the induced magnetism. The present work will in general help to tune the oxygen vacancy induced magnetic ordering in prototype systems.

#### ACKNOWLEDGMENTS

Authors acknowledge Dr. V. Raghavendra Reddy for RSM; Mr. Tarachand Patel and Dr. Gunadhor Okram

for resistivity, Mr. Avinash Wadikar, Mr. Sharad Karwal and Mr. Rakesh Sah for helping in measurements using synchrotron beamline at Indus - I & II, RRCAT, India. SM would like to thank Mr. Gyanendra Panchal and Mr. Anupam Jana for providing necessary discussions. PB acknowledges UGC, India, for the junior research fellowship [grant no. 20/12/2015(ii)EU- V]. PB and SB acknowledge the High Performance Computing (HPC) facility at IIT Delhi for computational resources. SB acknowledges the financial support from YSS-SERB research grant, DST, India (grant no. YSS/2015/001209).

#### REFERENCES

- [1] A. P. Chen, H. H. Zhou, Z. X. Bi, Y. Y. Zhu, Z. P. Luo, A. Bayraktaroglu, J. Phillips, E.-M. Choi, J. L. MacManus-Driscoll, S. J. Pennycook, J. Narayan, Q. Jia, X. Zhang, and H. Wang, A New Class of Room-Temperature Multiferroic Thin Films with Bismuth-Based Supercell Structure, *Adv. Mater.* **25** (2013) 1028.
- [2] B. J. Kennedy, G. Murphy, E. Reynolds, M. Avdeev, H. E. R. Brand and T. Kolodiaznyi, Studies of the antiferrodistortive transition in  $\text{EuTiO}_3$ , *J. Phys.: Condens. Matter* **26** (2014) 495901.
- [3] T. Shimada, Y. Uratani, T. Kitamura, Emergence of ferromagnetism at a vacancy on a non-magnetic ferroelectric  $\text{PbTiO}_3$  surface: A first-principles study, *Acta Materialia* **60** (2012) 6322-6330.
- [4] S.-Y. Chung, D. Y. Yoon, S.-Joong, L. Kang, Effects of donor concentration and oxygen partial pressure on interface morphology and grain growth behavior in  $\text{SrTiO}_3$ , *Acta Materialia* **50** (2002) 3361-3371.
- [5] Y. L. Zhu, M. J. Zhuo, X. L. Ma, and H. B. Lu, Microstructural characteristics in the  $\text{BaTiO}_{2.52}$  thin films showing metallic behavior, *Materials Letters* **61** (2007) 1971-1973.
- [6] Y. L. Li, S. Choudhury, J. H. Haeni, M. D. Biegalski, A. Vasudevarao, A. Sharan, H. Z. Ma, J. Levy, V. Gopalan, S. Trolier-McKinstry, D. G. Schlom, Q. X. Jia, and L. Q. Chen, Phase transitions and domain structures in strained pseudocubic (100)  $\text{SrTiO}_3$  thin films, *Phys. Rev. B* **73** (2006) 184112.
- [7] A. P. Chen, F. Khatkhatay, W. Zhang, C. Jacob, L. Jiao, and H. Wang, Strong oxygen pressure dependence of ferroelectricity in  $\text{BaTiO}_3/\text{SrRuO}_3/\text{SrTiO}_3$  epitaxial heterostructures, *J. Appl. Phys.* **114** (2013) 124101.
- [8] J. Xing, K.-J. Jin, H. Lu, M. He, G. Liu, J. Qiu and G. Yang, Photovoltaic effects and its oxygen content dependence in  $\text{BaTiO}_3\text{-}\delta/\text{Si}$  heterojunctions, *Appl. Phys. Lett.* **92** (2008) 071113.
- [9] J. Shieh, K.C. Wu, C.S. Chen, Switching characteristics of MPB compositions of  $(\text{Bi}_{0.5}\text{Na}_{0.5})\text{TiO}_3\text{-BaTiO}_3\text{-(Bi}_{0.5}\text{K}_{0.5})\text{TiO}_3$  lead-free ferroelectric ceramics, *Acta Materialia* **55** (2007) 3081-3087.
- [10] L. Qiao, X. Bi, Microstructure and ferroelectric properties of  $\text{BaTiO}_3$  films on  $\text{LaNiO}_3$  buffer layers by rf sputtering, *Journal of Crystal Growth* **310** (2008) 2780-2784.
- [11] Liao W. Q., Tang Y. Y., Li P. F., You Y. M., and Xiong R. G., Large Piezoelectric Effect in a Lead-Free Molecular Ferroelectric Thin Film, *J. Am. Chem. Soc.* **139** (2017) 18071-18077.
- [12] X.G. Tang, K.-H. Chew, H.L.W. Chan, Diffuse phase transition and dielectric tunability of  $\text{Ba}(\text{Zr}_{1-y}\text{Ti}_y)\text{O}_3$  relaxor ferroelectric ceramics, *Acta Materialia* **52** (2004) 5177-5183.
- [13] Zhou Z., Tang H., and Sodano H. A., Vertically Aligned Arrays of  $\text{BaTiO}_3$  Nanowires, *ACS Appl. Mater. Interfaces* **5** (2013) 11894-11899.
- [14] Y. Yano, K. Iijima, Y. Daitoh, T. Terashima, Y. Bando, Y. Watanabe, H. Kasatani, H. Terauchi, Epitaxial growth and dielectric properties of  $\text{BaTiO}_3$  films on Pt electrodes by reactive evaporation, *J. Appl. Phys.* **76** (1994) 7833.
- [15] F. Liu, I. Fina, G. Sauthier, F. Sánchez, A. M. Rappe and Josep Fontcuberta, Control of the Polarization of Ferroelectric Capacitors by the Concurrent Action of Light and Adsorbates, *ACS Appl. Mater. Interfaces* **10** (2018) 23968-23975.
- [16] Parizi S. S., Mellinger A., and Caruntu G., Ferroelectric Barium Titanate Nanocubes as Capacitive Building Blocks for Energy Storage Applications, *ACS Appl. Mater. Interfaces* **6** (2014) 17506-17517.
- [17] Sangsub Kim, Shunichi Hishita, Growing  $\text{BaTiO}_3$  thin films on Si(100) with MgO-buffer layers by sputtering, *Thin Solid Films* **449** (1996) 281-282.
- [18] D.J. Towner, J. Ni, T.J. Marks, B.W. Wessels, Effects of two-stage deposition on the structure and properties of heteroepitaxial  $\text{BaTiO}_3$  thin films, *J. Crystal Growth* **255** (2003) 107-113.
- [19] C L Li, Z H Chen, Y L Zhou and D F Cui, Effect of oxygen content on the dielectric and ferroelectric properties of laser-deposited  $\text{BaTiO}_3$  thin films, *J. Phys.: Condens. Matter* **13** (2001) 5261-5268.
- [20] Shin S. H., Seong-Young Choi S. Y., Lee M. H., and Nah J., High-Performance Piezoelectric Nanogenerators via Imprinted Sol-Gel  $\text{BaTiO}_3$  Nanopillar Array, *ACS Appl. Mater. Interfaces* **9** (2017) 41099-41103.
- [21] Suo G., Yu Y., Zhang Z., Wang S., Zhao P., Li J., and Wang X., Piezoelectric and Triboelectric Dual Effects in Mechanical-Energy Harvesting Using  $\text{BaTiO}_3/\text{Polydimethylsiloxane}$  Composite Film, *ACS Appl. Mater. Interfaces* **8** (2016) 34335-34341.
- [22] Yan J. and Jeong Y. G., High Performance Flexible Piezoelectric Nanogenerators based on  $\text{BaTiO}_3$  Nanofibers in Different Alignment Modes, *ACS Appl. Mater. Interfaces* **8** (2016) 15700-15709.
- [23] Yuji O., and Yoshikazu S., Perovskite-type  $\text{SrTiO}_3$ ,  $\text{CaTiO}_3$  and  $\text{BaTiO}_3$  porous film electrodes for dye-sensitized solar cells, *Journal of the Ceramic Society of Japan* **122**[8] (2014) 728-731.
- [24] Yuji O., and Yoshikazu S., Double-layer dye-sensitized solar cells using  $\text{SrTiO}_3$  and  $\text{BaTiO}_3$  second layer with enhanced photovoltaic performance, *Journal of the Ceramic Society of Japan* **123**[10] (2015) 967-971.
- [25] Hatameh A. M., Mohammad R. M.,  $\text{TiO}_2\text{-BaTiO}_3$  nanocomposite for electron capture in dye-sensitized solar cells, *J Am Ceram Soc.* (2017) 1-10.
- [26] L. Zhang, Y. Shi, S. Peng, J. Liang, Z. Tao, J. Chen, Dye-sensitized solar cells made from  $\text{BaTiO}_3$ -coated  $\text{TiO}_2$  nanoporous electrodes, *Journal of Photochemistry and Photobiology A: Chemistry* **197** (2008) 260-265.
- [27] Zhao G., Zhang X., Cui X., Wang S., Liu Z., Deng L., Qi A., Qiao X., Li L., Pan C., Zhang Y., and Li L., Piezoelectric Polyacrylonitrile Nanofiber Film-Based Dual-Function Self-Powered Flexible Sensor, *ACS Appl. Mater. Interfaces* **10** (2018) 15855-15863.
- [28] A. Raeliarijaona and H. Fu, Ferromagnetism in ferroelectric  $\text{BaTiO}_3$  induced by vacancies: Sensitive dependence on charge state, origin of magnetism, and temperature range of existence, *Phys. Rev. B* **96** (2017) 144431.
- [29] D. Cao, M. Q. Cai, Yue Zheng and W. Y. Hu, First-principles study for vacancy-induced magnetism in non-magnetic ferroelectric  $\text{BaTiO}_3$ , *Phys. Chem. Chem. Phys.* **11** (2009) 10934-10938.
- [30] Dan Cao, Meng-Qiu Cai, Wang-Yu Hu, Ping Yu and Hai-Tao Huang, Vacancy-induced magnetism in  $\text{BaTiO}_3(001)$

- thin films based on density functional theory, *Phys. Chem. Chem. Phys.* **13** (2011) 4738-4745.
- [31] Eom K., Choi E., Choi M., Han S., Zhou H., and Lee J., Oxygen Vacancy Linear Clustering in a Perovskite Oxide, *J. Phys. Chem. Lett.* **8**(15) (2017) 3500-3505.
- [32] A. Sundaresan and C. N. R. Rao, *Nano Today* **4** (2009) 96.
- [33] R. V. K. Mangalam, M. Chakrabarti, D. Sanyal, A. Chakrabati, and A. Sundaresan, *J. Phys.: Condens. Matter* **21** (2009) 445902.
- [34] F. Yang, H. Jin, H. Lu, M. He, C. Wang, J. Wen, and G. Yang, *Sci. China Phys. Mechanics & Astronomy* **53** (2010) 852.
- [35] D. Qin, Z. Liu, Y. Zuo, X. Sang, F. Zhang, F. Zheng, H. Liu, and X. Xu, *J. Phys. Chem. Lett.* **1** (2010) 238.
- [36] M. Wang, G. L. Tan, and Q. Zhang, *J. Amer. Ceram. Soc.* **93** (2010) 2151.
- [37] S. G. Bahoosh, S. Trimper, and J. M. Wesselinowa, Origin of ferromagnetism in BaTiO<sub>3</sub> nanoparticles, *Phys. Status Solidi RRL* **5** 10-11 (2011) 382-384.
- [38] H. Liu, B. Cao, and C. O'Connor, *J. Appl. Phys.* **109** (2011) 07B516.
- [39] S Ramakanth and K C James Raju, Charge transfer induced magnetism in nano crystalline BaTiO<sub>3</sub>, *Solid State Commun.* **187** (2014) 59.
- [40] G. Kresse and J. Furthmuller, Efficiency of ab-initio total energy calculations for metals and semiconductors using a plane-wave basis set, *Computational Materials Science* **6** (1996) 15-50.
- [41] G. Kresse and D. Joubert, From ultrasoft pseudopotentials to the projector augmented-wave method, *Phys. Rev. B* **59** (1999) 1758-1775.
- [42] J. P. Perdew and Y. Wang, Accurate and simple analytic representation of the electron-gas correlation energy, *Phys. Rev. B* **45** (1992) 13244-13249.
- [43] J. P. Perdew, K. Burke and M. Ernzerhof, Generalized Gradient Approximation Made Simple, *Phys. Rev. Lett.* **77** (1996) 3865-3868.
- [44] H. J. Monkhorst and J. D. Pack, Special points for Brillouin-zone integrations, *Phys. Rev. B* **13** (1976) 5188-5192.
- [45] W. Lia, F. Lua, Z.-G. Liub, Y. Zhuc, F.-X. Wanga, X.-D. Liua, C.-Y. Tana, K.-M. Wang, Quantitative analysis of the oxygen content in BaTiO<sub>3</sub> films deposited by PLD using <sup>16</sup>O( $\alpha$ ,  $\alpha'$ )<sup>16</sup>O resonant elastic scattering, *Thin Solid Films* **340** (1999) 68-71.
- [46] S. Hashimoto, T. Sugie, Z. Zhang, K. Yamashita and M. Noda, Effects of final annealing in oxygen on characteristics of BaTiO<sub>3</sub> thin films for resistance random access memory, *Jpn. J. Appl. Phys.* **54** (2015) 10NA12.
- [47] Komal Bapna, D. M. Phase, and R. J. Choudhary, Study of valence band structure of Fe doped anatase TiO<sub>2</sub> thin films, *J. Appl. Phys.* **110** (2011) 043910.
- [48] L. T. Hudson, R. L. Kurtz, S. W. Robey, D. Temple and R. L. Stockbauer, Photoelectron spectroscopic study of the valence and core-level electronic structure of BaTiO<sub>3</sub>, *Phys. Rev. B* **47** (1993-I) Number 3.
- [49] S. W. Robey, L. T. Hudson, V. E. Henrich, C. Eylem and B. Eichhorn, RESONANT PHOTOELECTRON SPECTROSCOPY STUDIES OF BaTiO<sub>3</sub> AND RELATED MIXED OXIDES, *J Phys. Chem Solids* **57** (1996) No. 10, pp. 1385-1391.
- [50] Komal Bapna, R. J. Choudhary, S. K. Pandey, D. M. Phase, S. K. Sharma and M. Knobel, Electronic depiction of magnetic origin in undoped and Fe doped TiO<sub>2</sub>-d epitaxial thin films, *Appl. Phys. Lett.* **99** (2011) 112502.
- [51] M. F. M. de Groot, M. Grioni, J. C. Fuggle, J. Ghijsen and G. A. Sawatzky, Oxygen 1s X-ray absorption edges of transition metal oxides, *Phys. Rev. B* **40** (1989-I) No. 8.
- [52] V.R. Mastelaro, H.R. Favarim, A. Mesquita, A. Michalowicz, J. Moscovici and J.A. Eiras, Local structure and hybridization states in Ba<sub>0.9</sub>Ca<sub>0.1</sub>Ti<sub>1-x</sub>Zr<sub>x</sub>O<sub>3</sub> ceramic compounds: Correlation with a normal or relaxor ferroelectric character, *Acta Materialia* **84** (2015) 164-171.
- [53] Jin Suntivich, Wesley T. Hong, Yueh-Lin Lee, James M. Rondinelli, Wanli Yang, John B. Goodenough, Bogdan Dabrowski, John W. Freeland, and Yang Shao-Horn, Estimating Hybridization of Transition Metal and Oxygen States in Perovskites from O Kedge X-ray Absorption Spectroscopy, *J. Phys. Chem. C* **118** (2014) 1856-1863.
- [54] A. E. Bocquet, T. Mizokawa, T. Saitoh, H. Namatame and A. Fujimori, Electronic structure of 3d-transition-metal compounds by analysis of the 2p core-level photoemission spectra, *Phys. Rev. B* **46** (1992) 3771-3784.
- [55] V. R. Galakhov, E. Z. Kurmaev, K. Kuepper, M. Neumann, J. A. McLeod, A. Moewes, I. A. Leonidov and V. L. Kozhevnikov, Valence Band Structure and X-ray Spectra of Oxygen-Deficient Ferrites SrFeO<sub>x</sub>, *J. Phys. Chem. C* **114** (2010) 5154-5159.
- [56] T. Kolodiazny, M. Tachibana, H. Kawaji, J. Hwang, and E. Takayama-Muromachi, Persistence of Ferroelectricity in BaTiO<sub>3</sub> through the Insulator-Metal Transition, *Phys. Rev. L* **104** (2010) 147602.
- [57] K. Maiti and D. D. Sarma, Spectroscopic investigations of the electronic structure and metal-insulator transitions in a Mott-Hubbard system La<sub>1-x</sub>CaxVO<sub>3</sub>, *Phys. Rev. B* **61** (2000-II) No. 4.
- [58] Weiwei Li, Run Zhao, Le Wang, Rujun Tang, Yuanyuan Zhu, Joo Hwan Lee, Haixia Cao, Tianyi Cail, Haizhong Guo, Can Wang, Langsheng Ling, Li Pi, Kuijuan Jin, Yuheng Zhang, Haiyan Wang, Yongqiang Wang, Sheng Ju1 & Hao Yang, Oxygen-Vacancy-Induced Antiferromagnetism to Ferromagnetism Transformation in Eu<sub>0.5</sub>Ba<sub>0.5</sub>TiO<sub>3</sub>-d Multiferroic Thin Films, *Sci. Rep.* **3** (2013) 2618.
- [59] H. Z. Guo et al., Influence of defects on structural and magnetic properties of multifunctional La<sub>2</sub>NiMnO<sub>6</sub> thin films, *Phys. Rev. B* **77** (2008) 174423.
- [60] Y. Tokura, Y. Taguchi, Y. Okada, Y. Fujishima, and T. Arima, K. Kumagai, Y. Iye, Filling Dependence of Electronic Properties on the Verge of Metal-Mott-Insulator Transitions in Sr<sub>1-x</sub>LaxTiO<sub>3</sub>, *Phys. Rev. Lett.* **70** (1993) 2126.
- [61] K. Kumagai, T. Suzuki, Y. Taguchi, Y. Okada, Y. Fujishima, and Y. Tokura, Metal-insulator transition in La<sub>1-x</sub>SrxTiO<sub>3</sub> and Y<sub>1-x</sub>CaxTiO<sub>3</sub> investigated by specific-heat measurements, *Phys. Rev. B* **48** (1993) 7636.
- [62] Yuan-Hua Lin, Jiancong Yuan, Songyin Zhang, Yi Zhang, Jing Liu, Yao Wang, and Ce-Wen Nan, Multiferroic behavior observed in highly orientated Mn-doped BaTiO<sub>3</sub> thin films, *Appl. Phys. Lett.* **95** (2009) 033105.
- [63] J. M. D. Coey, M. Venkatesan and C. B. Fitzgerald, Donor impurity band exchange in dilute ferromagnetic oxides, Temperature-dependent magnetization and susceptibility of Fe<sub>n</sub>/V<sub>7</sub> superlattices, *Nature materials* **4** (2005) 173-179.



- [64] J. Padilla and D. Vanderbilt, Ab initio study of BaTiO<sub>3</sub> surfaces, *Phys. Rev. B* **56** (1997) 1625.